

Regularized integral equation methods for elastic scattering problems in three dimensions

Oscar P. Bruno* and Tao Yin†

October 1, 2019

Abstract

This paper presents novel methodologies for the numerical simulation of scattering of elastic waves by both closed and open surfaces in three-dimensional space. The proposed approach utilizes new integral formulations as well as an extension to the elastic context of the efficient high-order singular-integration methods [12] introduced recently for the acoustic case. In order to obtain formulations leading to iterative solvers (GMRES) which converge in small numbers of iterations we investigate, theoretically and computationally, the character of the spectra of various operators associated with the elastic-wave Calderón relation—including some of their possible compositions and combinations. In particular, by relying on the fact that the eigenvalues of the composite operator NS are bounded away from zero and infinity, new uniquely-solvable, low-GMRES-iteration integral formulation for the closed-surface case are presented. The introduction of corresponding low-GMRES-iteration equations for the open-surface equations additionally requires, for both spectral quality as well as accuracy and efficiency, use of weighted versions of the classical integral operators to match the singularity of the unknown density at edges. Several numerical examples demonstrate the accuracy and efficiency of the proposed methodology.

Keywords: Elastic waves, combined field integral equations, Calderón relation, hyper-singular operator, high-order methods

1 Introduction

This paper introduces efficient high-order integral solvers for three-dimensional (3D) problems of elastic scattering by surfaces, including both *closed surfaces* and *infinitely thin open surfaces*. These are problems of significant importance in many application fields in science and engineering, including geophysics, seismology, non-destructive testing, energy and material science, among many others. Unlike the finite-element and finite-difference approximations of the associated partial differential equations [7], which require 3D (volumetric) discretizations and use of appropriate absorbing boundary conditions, the boundary integral methods only require discretization of the two-dimensional (2D) domain boundaries [21, 26, 27, 33] and they automatically enforce the radiation condition at infinity. The significant benefits inherent in the reduced dimensionality of the boundary-integral methods can be fully realized, in spite of the dense matrices they entail, provided adequate acceleration techniques are used for the associated matrix-vector products (see e.g. [11, 15, 29] and references therein) together with Krylov-subspace linear algebra solver like GMRES. In all, the BIE method has lead to fast and high-order algorithms that, for problems beyond a small number of wavelengths in size, can outperform their volumetric domain discretization counterparts to very significant extents.

For definiteness, this contribution focuses on the elastic Neumann (traction) boundary-value problem, whose treatment by means of boundary integral methods has been found quite challenging, but the

*Department of Computing & Mathematical Sciences, California Institute of Technology, 1200 East California Blvd., CA 91125, United States. Email: obruno@caltech.edu

†Department of Computing & Mathematical Sciences, California Institute of Technology, 1200 East California Blvd., CA 91125, United States. Email: taoyin89@caltech.edu

proposed methods extend directly to the somewhat less challenging elastic problems with Dirichlet (displacement) boundary conditions. For the Neumann problem of scattering by closed-surfaces the proposed method represents the elastic-field on the basis of a combination of single-layer and double-layer potentials [21], which ensures the validity of the critical property of unique solvability; the resulting integral equation includes contributions from the tractions of both the single-layer and double-layer potentials—which result in strongly singular and hyper-singular kernels, respectively, and which, unlike the single layer operator (whose kernel is weakly singular), are only defined in the sense of Cauchy principle value and Hadamard finite part [26], respectively. For the problem of scattering by open-surfaces, in turn, a representation leading to a hyper-singular integral operator is used [2, 20]. In both cases we propose an efficient high-order singular-integration method that extends the “rectangular-polar” methodology [12] introduced recently for the acoustic case, and which, as demonstrated below in this paper, can efficiently produce solutions of very high accuracy.

The presence of the elastic hyper-singular operator in the integral-equation formulations presents difficulties concerning spectral character and accurate operator evaluation, both of which arise from the highly singular character of the associated integral kernel. Indeed, as it is well known, the eigenvalues of the hyper-singular operators accumulate at infinity and, hence, the solution of these integral equations by means of the GMRES solver often requires large numbers of iterations for convergence—and thus, large computing costs, specially for 3D problems. On the other hand, the very evaluation of the associated hyper-singular integrals for both open- and closed-surface problems, that must be interpreted in the sense of Hadamard finite part, has also remained a significant challenge [17, 26]. When combined with the iterative linear-algebra solver GMRES, the proposed combination of a spectrally regularized formulation and novel and effective high-order singular quadratures gives rise to efficient and highly accurate solvers for the elastic-wave problems at hand. We suggest that the use of the aforementioned acceleration techniques, which can directly be applied in conjunction with the formulation and singular-quadrature methods presented in this paper, would lead to accurate and efficient solvers for high-frequency elastic-scattering problems as well.

A number of strategies have been developed, in the context of acoustic and electromagnetic scattering, for reduction of the number of GMRES iterations required for convergence to a given accuracy. Unlike the algebraic preconditioners [10, 18] and formulations based on pseudoinverses [5, 6], the novel methodologies proposed in [11] rely on the acoustic Calderón relation and only require use of a regularizing operator of a form similar to a single-layer operator, leading to regularized integral equations that are of the desired second-kind Fredholm type. In both cases the regularization technique preserves the unique solvability properties of the classical (unregularized) integral equations upon which they are based.

The extension of these methodologies to elastic scattering problems presents certain challenges. At a basic level, elastic-wave Calderón formulas have not been studied in detail for either closed-surface or open-surface cases—possibly on account of the fact that, in contrast with the acoustic wave case, the classical double-layer operator K and its adjoint K' (which play important roles in the Calderón relations) are not compact in the elastic case [3, 4]. The 2D elastic Calderón formula for the closed-surface case was investigated recently [16]. On the basis of the polynomial compactness of the operators K and K' it was shown that the composition NS of the single-layer and hyper-singular integral operators can be expressed as the sum of a multiple of the identity operator and a compact operator. The closed-surface 2D analysis does not directly translate to the 3D context in view of certain differences in the detailed character of the polynomial compactness of the operators K and K' in the 3D [4] and 2D [3] cases, but, as shown in Section 3, the eigenvalues of the composition NS in 3D are bounded away from zero and infinity. Analyses based on principal symbols, such as the one presented in [23] for the on-surface radiation-condition regularization method in the Dirichlet case, could conceivably be applied to study the spectral regularity of the three-dimensional elastic operator NS , but such approaches have not as yet been pursued. We are not aware of previous applications of spectral regularization methods to integral equations for the elastic Neumann problem.

Elastic versions of the Calderón formulas for open surfaces are not known at present. In view of the acoustic open-surface Calderón relations [13, 14, 28] and the related study [16] for the 2D open-arc elastic case, we consider “weighted” versions S_w and N_w of the single-layer and hyper-singular operators which,

like those considered previously for 2D elastic and 2D and 3D acoustic open surface problems, extract the solutions' edge singularity explicitly. In view of these contributions and the spectral properties, established in the present paper for the 3D closed-surface elastic case, we additionally consider a formulation of the 3D open-surface elastic problem in terms of the composition $N_w S_w$. The benefits of this approach are two-fold: high-order accuracy (that is achieved in our implementations by means of the aforementioned rectangular-polar quadrature method) and well-behaved iterative linear algebra. Our numerical tests suggest that the eigenvalues of $N_w S_w$ are at least bounded away from infinity, and although they appear to approach the origin (Fig.3), the $N_w S_w$ formulation leads, as desired, to significant reductions in the number of GMRES iterations required for convergence to a given residual tolerance over those required by the operator N_w .

As indicated above, our implementations rely on the Chebyshev-based rectangular-polar discretization methodology developed recently [12]—which can be readily applied in conjunction with geometry descriptions given by a set of arbitrary non-overlapping logically-quadrilateral patches, and which, therefore, makes the algorithm particularly well suited for treatment of complex CAD-generated geometries. The algorithms additionally rely on use of expressions, presented in [9, 31, 36] for the closed-surface case, that present 3D elastic strongly-singular and hyper-singular operators as compositions of weakly singular integrals and tangential-derivative operators; the corresponding expressions for the weighted operators we use in the open-surface case are presented in Lemma 3.5 below. The application of the Chebyshev-based rectangular-polar solver for the evaluation of the weakly singular integrals gives rise to high accuracy and efficiency. Thanks to the use of Cartesian-product Chebyshev discretizations, further, the needed tangential differentiations can easily be effected via differentiation of corresponding truncated Chebyshev expansions.

This paper is organized as follows. After preliminaries and notations are laid down in Section 2.1, Sections 2.2 and 2.3 introduce the classical integral equations for the closed-surface and open-surface problems under consideration, respectively. Section 3.1 investigates the spectral properties of the elastic integral operators and the 3D Calderón relation. The new regularized integral equations for closed and open surfaces are derived in Sections 3.2 and 3.3, respectively. Exact re-expressed formulations for the strongly-singular and hyper-singular operators are presented in Section 3.4. The high order discretization method we use for numerical evaluation of the elastic integral operators are briefly described in Section 4. The numerical examples presented in Section 5, finally, demonstrate the high-accuracy and high-order of convergence enjoyed by the proposed approach, as well as the reduced numbers of GMRES linear-algebra iterations required by the proposed algorithms for convergence to a given residual tolerance.

2 Elastic scattering problems and integral equations

2.1 Preliminaries

We consider the problems of scattering of elastic waves by bounded obstacles Ω whose smooth boundaries Γ are either open or closed surfaces—that is, they are two-dimensional sub-manifolds of \mathbb{R}^3 with or without boundary, respectively. Noting that in the open-surface case we have $\Omega = \Gamma$, for both the open and closed-surface cases the propagation domain will be denoted by $D := \mathbb{R}^3 \setminus \overline{\Omega}$. We assume that D is occupied by a linear isotropic and homogeneous elastic medium characterized by the Lamé constants λ and μ (satisfying $\mu > 0$, $3\lambda + 2\mu > 0$) and the mass density $\rho > 0$. As indicated in Section 1, our derivations are restricted to the challenging Neumann case, in which the boundary traction is prescribed. Suppressing the time-harmonic dependence $e^{-i\omega t}$ in which $\omega > 0$ is the frequency, the displacement field $u = (u^1, u^2, u^3)^\top$ in the solid (where a^\top denotes transposition of the vector or matrix a) can be modeled by the following boundary value problem: Given the boundary data F on Γ , determine the scattered field u satisfying

$$\Delta^* u + \rho\omega^2 u = 0 \quad \text{in } D, \tag{2.1}$$

$$T(\partial, \nu)u = F \quad \text{on } \Gamma, \tag{2.2}$$

and the Kupradze radiation condition ([27])

$$\lim_{r \rightarrow \infty} r \left(\frac{\partial u_t}{\partial r} - ik_t u_t \right) = 0, \quad r = |x|, \quad t = p, s, \quad (2.3)$$

uniformly with respect to all $\hat{x} = x/|x| \in \mathbb{S}^2 := \{x \in \mathbb{R}^3 : |x| = 1\}$. Here, Δ^* denotes the Lamé operator

$$\Delta^* := \mu \operatorname{div} \operatorname{grad} + (\lambda + \mu) \operatorname{grad} \operatorname{div},$$

and $T(\partial, \nu)$ denotes the boundary-traction operator

$$T(\partial, \nu)u := 2\mu \partial_\nu u + \lambda \nu \operatorname{div} u + \mu \nu \times \operatorname{curl} u, \quad \nu = (\nu^1, \nu^2, \nu^3)^\top,$$

where ν is the outward unit normal to the boundary Γ and $\partial_\nu := \nu \cdot \operatorname{grad}$ is the normal derivative. In (2.3), u_p and u_s denote the compressional and the shear waves, respectively, which are given by

$$u_p = -\frac{1}{k_p^2} \operatorname{grad} \operatorname{div} u, \quad u_s = \frac{1}{k_s^2} \operatorname{curl} \operatorname{curl} u,$$

where the wave numbers k_s, k_p are defined as

$$k_s := \omega/c_p, \quad k_p := \omega/c_s,$$

with

$$c_p := \sqrt{\mu/\rho}, \quad c_s := \sqrt{(\lambda + 2\mu)/\rho}.$$

If the scattered field is induced by an incident displacement field u^{inc} (e.g. a plane wave or point source), then the boundary data is determined by $F = -T(\partial, \nu)u^{inc}$.

The fundamental displacement tensor for the time-harmonic Navier equation (2.1) in \mathbb{R}^3 is given by

$$E(x, y) = \frac{1}{\mu} \gamma_{k_s}(x, y) I + \frac{1}{\rho \omega^2} \nabla_x \nabla_x^\top [\gamma_{k_s}(x, y) - \gamma_{k_p}(x, y)], \quad x \neq y, \quad (2.4)$$

where

$$\gamma_{k_t}(x, y) = \frac{\exp(ik_t|x-y|)}{4\pi|x-y|}, \quad x \neq y, \quad t = p, s. \quad (2.5)$$

is the fundamental solution of the Helmholtz equation in \mathbb{R}^3 with wave number k_t . Relying on the p -wave and s -wave Helmholtz Green functions (2.5), Sections 2.2 and 2.3 present the classical indirect boundary integral equations for the traction problems of scattering by closed and open surfaces, respectively.

2.2 Boundary integral equations I: closed-surface case

The classical indirect combined field integral equation formulation assumes a representation of the scattered field given by a combination of the form [26]

$$u(x) = (\mathcal{D} - i\eta \mathcal{S})(\varphi)(x), \quad x \in D, \quad (2.6)$$

of a single and a double-layer potential expressions \mathcal{D} and \mathcal{S} given by

$$\mathcal{D}(\varphi)(x) = \int_{\Gamma} (T(\partial_y, \nu_y)E(x, y))^\top \varphi(y) ds_y, \quad (2.7)$$

$$\mathcal{S}(\varphi)(x) = \int_{\Gamma} E(x, y)\varphi(y) ds_y, \quad (2.8)$$

respectively. Operating with the traction operator on (2.6), taking the limit as $x \rightarrow \Gamma$ and using well-known jump relations [26] to apply the boundary condition, the combined field integral equation

$$\left[i\eta \left(\frac{I}{2} - K' \right) + N \right] (\varphi) = F \quad \text{on } \Gamma \quad (2.9)$$

results. Here I denotes the identity operator, and $K' : H^s(\Gamma)^3 \rightarrow H^s(\Gamma)^3$ and $N : H^s(\Gamma)^3 \rightarrow H^{s-1}(\Gamma)^3$ denote the boundary integral operators

$$K'(\varphi)(x) = \int_{\Gamma} T(\partial_x, \nu_x) E(x, y) \sigma(y) ds_y, \quad x \in \Gamma, \quad \text{and} \quad (2.10)$$

$$N(\varphi)(x) = \int_{\Gamma} T(\partial_x, \nu_x) (T(\partial_y, \nu_y) E(x, y))^{\top} u(y) ds_y, \quad x \in \Gamma, \quad (2.11)$$

which are only defined in the sense of Cauchy principle value and Hadamard finite part [26] respectively, in view of the strongly singular and hyper-singular character of the corresponding kernels. It can be shown that the integral equation (2.9) is uniquely solvable for all real values of the frequency $\omega > 0$ (see e.g. [8]). But, as it is well known, the eigenvalues of the hypersingular integral operator N accumulate at infinity. As a result, the solution of the integral equation (2.9) by means of Krylov-subspace iterative solvers such as GMRES generally requires large numbers of iterations.

2.3 Boundary integral equations II: open-surface case

For the open-surface scattering problem the solution can be expressed as a double-layer potential

$$u(x) = \mathcal{D}(\varphi)(x), \quad x \in D. \quad (2.12)$$

Operating with the traction operator on (2.12), taking the limit as $x \rightarrow \Gamma$ and applying the boundary condition, we obtain the boundary integral equation

$$N(\varphi) = F \quad \text{on } \Gamma. \quad (2.13)$$

In addition to the computational challenge inherent in the accurate integration of the hypersingular kernel of the operator N , for the open-surface case the solution φ is itself singular at the edge of Γ , as is well known—which leads to numerical methods of low order of accuracy unless the algorithm appropriately accounts for the solution singularity.

3 Regularized boundary integral equations

In this section, we propose the regularized integral equations for the closed and open surface scattering problems. Here, three types of “regularization” are employed:

- I. *Form of integral equation regularization*: deriving new integral equations (Sections 3.2 and 3.3) on a basis of the spectral properties of the composition of single layer operator and hyper-singular operator (Section 3.1);
- II. *Solutions’ edge singularity regularization for open-surface cases*: introducing a weight function to extract the solutions’ edge singularity explicitly (Section 3.3);
- III. *Strong-singularity and hyper-singularity regularization*: Re-expressing the strongly singular and hyper-singular integral operators into compositions of weakly-singular integral operators and differentiation operators in directions tangential to the surface (Section 3.4).

3.1 Operator spectra

Seeking to derive regularized boundary integral equations which do not suffer from the difficulties described in the previous section, we first study the spectra of the integral operators K' and the composite operator NS where $S : H^s(\Gamma)^3 \rightarrow H^{s+1}(\Gamma)^3$ denotes the single-layer operator

$$S(\varphi)(x) = \int_{\Gamma} E(x, y)\sigma(y) ds_y, \quad x \in \Gamma. \quad (3.1)$$

Our study for wave-scattering problems relies on the following result for zero-frequency (static) elasticity.

Theorem 3.1. [4, Theorem 2.1, 2.2] *Let Γ denote a smooth closed surface in three-dimensional space, let K'_0 denote the adjoint of the elastic double-layer operator in the zero-frequency case $\omega = 0$ and let $P_3(t) = t(t^2 - C_{\lambda, \mu}^2)$ where $C_{\lambda, \mu}$ is a constant that depends on the Lamé parameters:*

$$C_{\lambda, \mu} = \frac{\mu}{2(\lambda + 2\mu)}.$$

Then $P_3(K'_0) : H^{-1/2}(\Gamma)^3 \rightarrow H^{-1/2}(\Gamma)^3$ is compact. Furthermore, the spectrum of K'_0 consists of three non-empty sequences of eigenvalues which converge to 0, $C_{\lambda, \mu}$ and $-C_{\lambda, \mu}$, respectively.

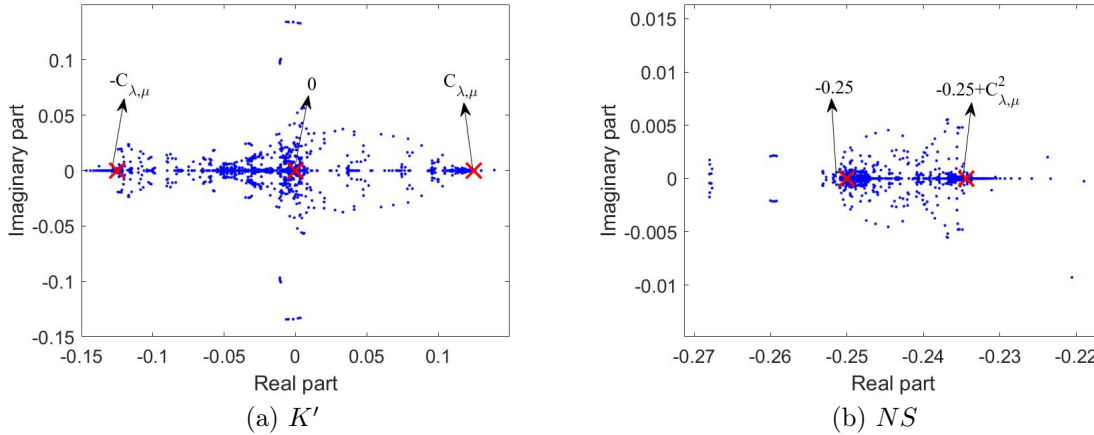


Figure 1: Eigenvalue distributions for the integral operators K' and NS .

Using this result we can explicitly obtain the accumulation points of the eigenvalues of K' . Indeed, since $K' - K'_0$ has a weakly-singular kernel it follows that $K' - K'_0$ is a compact operator, and we obtain

$$P_3(K') = P_3(K'_0) + K_c, \quad K_c = K'(K' - K'_0)(K' + K'_0) + (K' - K'_0)(K'^2_0 - C_{\lambda, \mu}^2 I),$$

where K_c is a compact operator. Therefore, the spectrum of K' also consists of three sequences of eigenvalues which converge to 0, $C_{\lambda, \mu}$ and $-C_{\lambda, \mu}$, respectively. In view of the Calderón relation [26]

$$NS = -\frac{I}{4} + K'^2, \quad (3.2)$$

together with the inequalities $0 < C_{\lambda, \mu} < 3/8$ (which result easily from the condition $\lambda + 2/3\mu > 0$) we conclude that the eigenvalues of the composite operator NS , which plays an essential role in the regularized integral equations proposed in the following section, are bounded away from zero and infinity.

To visualize the significance of these results we consider the integral operators K' and NS associated with the problem of scattering by a unit ball, and we choose $\lambda = 2$, $\mu = 1$, $\rho = 1$, $\omega = \pi$, from which

we obtain $C_{\lambda,\mu} = 0.125$. Letting N_{DOF} denote the number of degrees of freedom used for operator discretization, the eigenvalue distributions for the various operators, which were obtained numerically as the eigenvalues of the $N_{\text{DOF}} \times N_{\text{DOF}}$ matrices that result as each operator discretized on the basis of the method introduced in Section 4 with 6 patches, $N = 16$, $N^\beta = 100$ and $p = 8$, are displayed in Figure 1. (Matrices for the various operators were obtained by applying the discretized operators described in Section 4 to the canonical basis of $C^{N_{\text{DOF}}}$, and, for simplicity, the eigenvalues of the resulting matrices were obtained by means of Matlab’s function *eig*.)

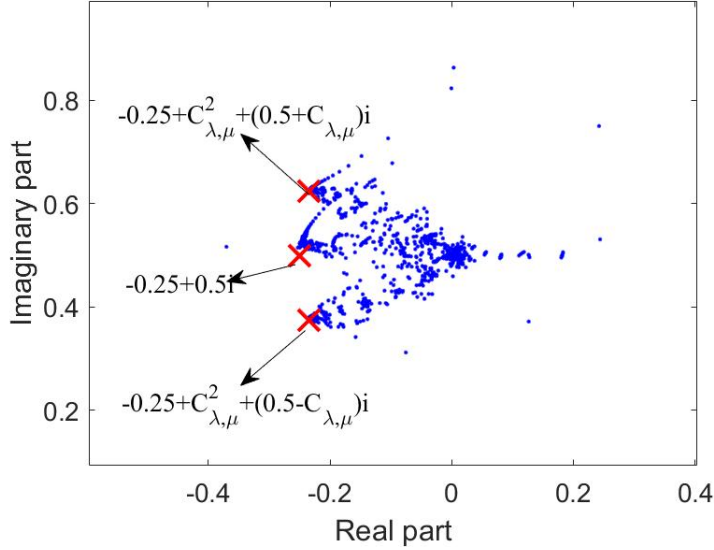


Figure 2: Eigenvalue distribution for the integral operator $i\left(\frac{I}{2} - K'\right) + N\mathcal{R}$ in (3.4).

3.2 Regularized boundary integral equation I: closed-surface case

Relying on the studies presented in Section 3.1 of the spectra of various relevant elastic-scattering integral operators, this section proposes regularized combined field equations that make use of the single-layer operator $\mathcal{R} := S_{i\omega_1}$ ($\omega_1 > 0$) for the “imaginary-frequency” $i\omega_1$ —in addition to the aforementioned double-layer and hypersingular operators K' and N . For simplicity, we assume $\omega_1 = \omega$. Thus, replacing the scattered field representation (2.6) by the expression

$$u(x) = (\mathcal{D}\mathcal{R} - i\eta\mathcal{S})(\psi)(x), \quad x \in D, \quad (3.3)$$

we obtain the regularized integral equation

$$\left[i\eta \left(\frac{I}{2} - K' \right) + N\mathcal{R} \right] (\psi) = F \quad \text{on } \Gamma, \quad (3.4)$$

instead of the classical combined field equation (2.9). The favorable properties of equation (3.4) are described in the following theorem.

Theorem 3.2. *The regularized integral equation (3.4) is uniquely solvable. The spectrum of the regularized combined field integral operator on the left hand side of that equation consists of three non-empty sequences of eigenvalues which converge to $-1/4 + C_{\lambda,\mu}^2 + i\eta(1/2 + C_{\lambda,\mu})$, $-1/4 + i\eta/2$ and $-1/4 + C_{\lambda,\mu}^2 + i\eta(1/2 - C_{\lambda,\mu})$, respectively.*

Proof. We need to show that the homogeneous equation of (3.4) only admits the trivial solution. Let us call u^+ (resp. u^-) the potential defined for $x \in D$ (resp. $x \in \Omega$) by the right hand side of Equation (3.3). Clearly, u^+ is a radiative solution to the elastic problem in D with $T(\partial, \nu)u^+ = 0$ on Γ . We conclude that $u^+ = 0$ everywhere outside Ω . From the classical jump relations for the boundary values of layer potentials, we see that

$$u^- = -S_{i\omega}(\psi), \quad T(\partial, \nu)u^- = i\eta\psi.$$

Applying Betti's formula [7], we then obtain

$$i\eta \int_{\Gamma} S_{i\omega}(\psi)\bar{\psi} ds = \int_{\Omega} \left(\frac{\mu}{2} |\nabla u^- + \nabla^{\top} u^-|^2 + \lambda |\nabla \cdot u^-|^2 - \rho\omega^2 |u^-|^2 \right) dx,$$

and therefore,

$$\int_{\Gamma} S_{i\omega}(\psi)\bar{\psi} ds = 0.$$

It is known that $S_{i\omega}$ is positive definite [1, Lemma 6.2], that is, there exists some positive constant $c > 0$ such that

$$\int_{\Gamma} S_{i\omega}(\psi)\bar{\psi} ds \geq c \|\psi\|_{H^{-1/2}(\Gamma)^3}^2.$$

This implies that $\psi = 0$ on Γ .

Noting that

$$i\eta \left(\frac{I}{2} - K' \right) + N\mathcal{R} = i\eta \left(\frac{I}{2} - K' \right) + NS + N(S_{i\omega} - S),$$

and since $(S_{i\omega} - S) : H^{-1/2}(\Gamma)^3 \rightarrow H^{1/2}(\Gamma)^3$ is a compact operator (in view of its kernel's smoothness), the claims concerning accumulation points of eigenvalue sequences of the combined integral operator (3.4) follows from the results presented in Section 3.1. The proof is now complete. \square

To illustrate Theorem 3.2 we utilize once again the unit-ball scattering problem considered in Section 3.1. The spectrum of the corresponding regularized combined field operator is displayed in Figure 2. Clearly the eigenvalues accumulate as prescribed by the theorem, and, in particular, they do not accumulate either at zero or infinity.

3.3 Regularized boundary integral equation II: open-surface case

In our treatment of an open surface Γ we assume, for simplicity, that the surface Γ , its edge, and the right hand side in equation (2.13) are infinitely smooth. Under such assumptions, the singular character of the solution φ is given by [22]

$$\varphi = \psi d^{1/2},$$

where ψ is an infinitely differentiable function in a neighborhood of the edge, up to and including the edge, and where d denotes the distance to the edge. In view of this result we introduce a weight function $w(x)$ which is smooth, positive and non-vanishing across the interior of the surface, and which, up to a factor that is C^∞ throughout Γ (including the edge) has square-root asymptotic edge behavior

$$w \sim d^{1/2} \quad \text{around the edge of } \Gamma.$$

Then we define the weighted operator

$$N_w(\psi) = N(w\psi), \tag{3.5}$$

so that for functions F that are smooth on Γ , up to and including the edge, the solution of the equation

$$N_w(\psi) = F \quad \text{on } \Gamma, \quad (3.6)$$

is also smooth throughout the surface. In view of the spectral properties of the closed-surface composite operator NS , we consider the composite operator $N_w S_w$ and the corresponding equation

$$N_w S_w(\psi) = F \quad \text{on } \Gamma. \quad (3.7)$$

Here S_w is a weighed version of the operator S ,

$$S_w(\psi) = S(\psi/w),$$

(which can also be used for treatment of the scattering problem under Dirichlet boundary conditions [13, 14, 16, 28]; see also Remark 3.3 and Figures 12 and 14 in Section 5).

As shown in [13, 28], the equation analogous to (3.7) for the 2D acoustic open-arc case is a second-kind equation. Further, the numerical results presented in [13, 14] for 2D/3D acoustic problems and in [16] for 2D elastic problems show that, in the cases considered in those contributions, equation (3.7) requires significantly smaller numbers of GMRES iterations than equation (3.6) for convergence to a given residual tolerance. For our numerical study of the spectrum of the operator $N_w S_w$ in the present elastic case we consider operators associated with the problem of elastic scattering by a unit disc (using the same parameters in Section 3.1). Figure 3 displays numerical values of the eigenvalues of the operator $N_w S_w$, which were obtained by applying the discretization method introduced in Section 4 with 5 patches. This figure clearly suggests that the eigenvalues of $N_w S_w$ are at least bounded away from infinity, although they also appear to approach the origin. As demonstrated in Figure 11, reduction in iteration numbers are observed for three-dimensional open-surface elastic problems that are analogous to those obtained for the corresponding closed-surface elastic case (Figures 5 through 7).

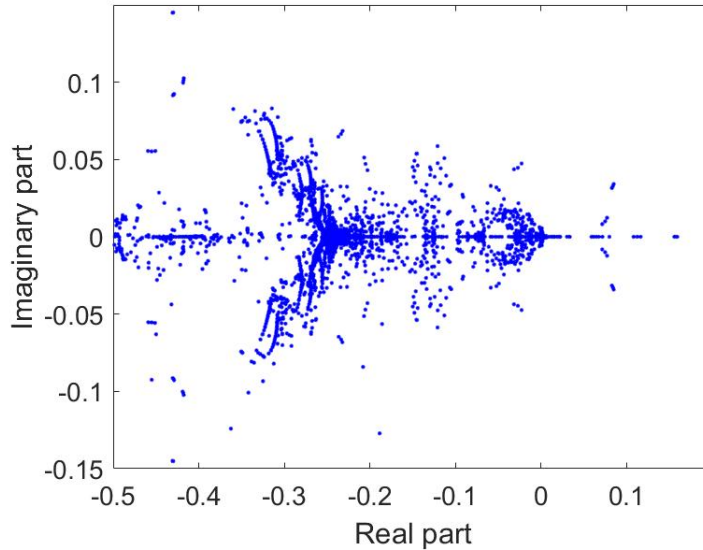


Figure 3: Eigenvalue distribution for the integral operator $N_w S_w$ in (3.7).

Remark 3.3. *The regularization techniques introduced for the Neumann problem can also be applied for the problems of scattering under Dirichlet boundary conditions*

$$u = G \quad \text{on } \Gamma.$$

For the Dirichlet problem the solution can be expressed as a single-layer potential

$$u(x) = \mathcal{S}(\varphi)(x), \quad x \in D,$$

which results in the boundary integral equation

$$S(\varphi) = G \quad \text{on } \Gamma.$$

The singular character of the solution φ , which is given by $\varphi \sim \psi d^{-1/2}$ [22] where ψ is an infinitely differentiable function throughout Γ , up to and including the edge, leads us to consider the weighted integral equation

$$S_w(\psi) = G \quad \text{on } \Gamma. \quad (3.8)$$

As in the Neumann case, further, we can also consider the combined operator $N_w S_w$ and the corresponding equation

$$N_w S_w(\psi) = N_w(G) \quad \text{on } \Gamma, \quad (3.9)$$

for the Dirichlet problem—although, as demonstrated in Figure 12, the single layer formulation (3.8) already requires small iteration numbers, and no improvements in iteration numbers result in this case from use of the $N_w S_w$ formulation.

3.4 Strong-singularity and hyper-singularity regularization

As noted in Sections 1, 2.2 and 2.3, the integral operators K' , N and N_w are strongly singular and hyper-singular, respectively. This section expresses the strongly singular and hyper-singular boundary integral operators (3.4) and (3.7) in terms of compositions of operators of differentiation in directions tangential to Γ and weakly-singular integral operators [9, 36]. Using this reformulation together with efficient numerical implementations of weakly-singular and tangential differentiation operators and the linear algebra solver GMRES then leads to the proposed elastic-wave solvers.

The traction operator can be expressed in the form

$$T(\partial, \nu)u(x) = (\lambda + \mu)\nu(\nabla \cdot u) + \mu\partial_\nu u + \mu M(\partial, \nu)u \quad (3.10)$$

where the operator $M(\partial, \nu)$, whose elements are also called Günter derivatives, is defined by

$$M(\partial, \nu)u(x) = \partial_\nu u - \nu(\nabla \cdot u) + \nu \times \text{curl } u.$$

Letting $M(\partial_x, \nu_x) = [m_x^{ij}]_{i,j=1}^3$, it is easy to check that

$$m_x^{ij} = \partial_{x_i} \nu_x^j - \partial_{x_j} \nu_x^i = -m_x^{ji} \quad \text{for } i, j = 1, 2, 3,$$

and

$$M(\partial, \nu) = \begin{pmatrix} 0 & -\tilde{\partial}_3 & \tilde{\partial}_2 \\ \tilde{\partial}_3 & 0 & -\tilde{\partial}_1 \\ -\tilde{\partial}_2 & \tilde{\partial}_1 & 0 \end{pmatrix},$$

where $\tilde{\partial}_i, i = 1, 2, 3$ are the components of $\nu \times \nabla$, i.e., $\nu \times \nabla = (\tilde{\partial}_1, \tilde{\partial}_2, \tilde{\partial}_3)^\top$. Let ∇^S denote the surface gradient:

$$\nabla^S u = \nabla u - \nu \partial_\nu u.$$

Then we have $\nu \times \nabla = \nu \times \nabla^S$. Writing $\nu \times \nabla^S = (\tilde{\partial}_1^S, \tilde{\partial}_2^S, \tilde{\partial}_3^S)^\top$, we obtain

$$M(\partial, \nu) = \begin{pmatrix} 0 & -\tilde{\partial}_3^S & \tilde{\partial}_2^S \\ \tilde{\partial}_3^S & 0 & -\tilde{\partial}_1^S \\ -\tilde{\partial}_2^S & \tilde{\partial}_1^S & 0 \end{pmatrix}.$$

The following lemma can be established as in [9], and we omit the proof here.

Lemma 3.4. *The boundary integral operator K' can be expressed in the form*

$$K' = K_1 + M(\partial, \nu)K_2, \quad (3.11)$$

where

$$\begin{aligned} K_1(\varphi)(x) &= \int_{\Gamma} \{ \partial_{\nu_x} \gamma_{k_s}(x, y)I - \nu_x \nabla_x^{\top} [\gamma_{k_s}(x, y) - \gamma_{k_p}(x, y)] \} \varphi(y) ds_y \quad \text{and} \\ K_2(\varphi)(x) &= \int_{\Gamma} [2\mu E(x, y) - \gamma_{k_s}(x, y)I] \varphi(y) ds_y. \end{aligned}$$

For the hyper-singular operator N , in turn, we have

$$N = N_1 + M(\partial, \nu)N_2M(\partial, \nu) + \mathcal{T}_2N_3\mathcal{T}_1 + M(\partial, \nu)N_4 + N_5M(\partial, \nu), \quad (3.12)$$

where

$$\begin{aligned} N_1(\varphi)(x) &= -\rho\omega^2 \int_{\Gamma} [\gamma_{k_s}(x, y)(\nu_x\nu_y^{\top} - \nu_x^{\top}\nu_yI) - \gamma_{k_p}(x, y)\nu_x\nu_y^{\top}] \varphi(y) ds_y, \\ N_2(\varphi)(x) &= \int_{\Gamma} [4\mu^2E(x, y) - 3\mu\gamma_{k_s}(x, y)I] \varphi(y) ds_y, \\ N_3(\varphi)(x) &= \mu \int_{\Gamma} \gamma_{k_s}(x, y)\varphi(y) ds_y, \\ N_4(\varphi)(x) &= \int_{\Gamma} \{ \mu\partial_{\nu_y} \gamma_{k_s}(x, y)I - 2\mu\nabla_y[\gamma_{k_s}(x, y) - \gamma_{k_p}(x, y)]\nu_y^{\top} \} \varphi(y) ds_y, \\ N_5(\varphi)(x) &= \int_{\Gamma} \{ \mu\partial_{\nu_x} \gamma_{k_s}(x, y)I - 2\mu\nu_x\nabla_x^{\top}[\gamma_{k_s}(x, y) - \gamma_{k_p}(x, y)] \} \varphi(y) ds_y, \end{aligned}$$

and where, for a scalar field v and a vector field V , the operators \mathcal{T}_1 and \mathcal{T}_2 in (3.12) are defined by

$$\mathcal{T}_1v = \nu \times \nabla^S v, \quad \mathcal{T}_2V = (\nu \times \nabla^S) \cdot V.$$

The kernels of the integral operators $K_i, i = 1, 2$ in (3.11) and $N_j, j = 1, \dots, 5$ in (3.12) are all at-most weakly-singular.

Noting that $w^2(x)$ is a smooth function of x throughout Γ which vanishes at the edge of Γ , the following open-surface version of the previous lemma can similarly be established.

Lemma 3.5. *The hyper-singular operator N_w can be expressed in the form*

$$N_w = N_1^w + M(\partial, \nu)N_2^w\mathcal{T}^w + \mathcal{T}_2N_3^w\mathcal{T}_1^w + M(\partial, \nu)N_4^w + N_5^w\mathcal{T}^w, \quad (3.13)$$

where

$$\begin{aligned} N_i^w(\varphi) &= N_i(w\varphi), \quad i = 1, 4, \\ N_j^w(\varphi) &= N_j(\varphi/w), \quad j = 2, 3, 5, \end{aligned}$$

and where, for a scalar field v and a vector field V , the operators \mathcal{T}_1^w and \mathcal{T}^w are given by

$$\mathcal{T}_1^w v = w^2\nu \times \nabla^S v + \frac{v}{2}\nu \times \nabla^S(w^2),$$

$$\mathcal{T}^w V = w^2M(\partial, \nu)V + M(\partial, \nu)(w^2)\frac{V}{2},$$

respectively. The kernels of the integral operators $N_j^w, j = 1, \dots, 5$ in (3.13) are all at-most weakly-singular.

4 Numerical implementation

In view of the integral-operator formulations presented in Section 3.4, a numerical version of the regularized integral operators introduced in Sections 2.2 and 3.3 can be obtained as a sum of (possibly multiple) compositions of numerical operators of two types, namely, (i) Integral operators of the forms

$$\mathcal{H}\varphi(x) = \int_{\Gamma} H(x, y)\varphi(y)ds_y, \quad (4.1)$$

$$\widehat{\mathcal{H}}^1(x) = \int_{\Gamma} H(x, y)\varphi(y)w(y)ds_y, \quad (4.2)$$

$$\widehat{\mathcal{H}}^2(x) = \int_{\Gamma} H(x, y)\varphi(y)/w(y)ds_y, \quad (4.3)$$

in which the kernel $H(x, y)$ is weakly singular, and (ii) Differentiation operators for the evaluation of the surface gradient of a given smooth function defined on Γ . Here, the integral (4.1) is related to closed-surface problems and the integrals (4.2) and (4.3) are related to open-surface problems. This section presents algorithms for numerical evaluation of operators of these types, including a rectangular-polar [12] Chebyshev-based quadrature method for weakly singular operators \mathcal{H} , $\widehat{\mathcal{H}}^1$ and $\widehat{\mathcal{H}}^2$ as well as Chebyshev-based differentiation algorithms. In all, the regularized iterative open- and closed-surface solvers rely on

- (1). A partition of the scattering surface Γ into a set of non-overlapping logically-quadrilateral parametrized patches;
- (2). High-order integration rules based on Chebyshev polynomials, Fejer's first quadrature rule, and "rectangular-polar" changes of variables which produce accurate approximations of the integral operators with weakly-singular kernels;
- (3). Chebyshev-based differentiation rules; and,
- (4). The iterative linear algebra solver GMRES, for solution of the discrete versions of Eqs. (3.4) and (3.7).

The methods for evaluation of the weakly singular and differentiation operators in closed-surface cases differ somewhat from their open-surface counterparts. Accordingly, Sections 4.1 and 4.2 present algorithms for the tasks (1) through (3) above in the closed- and open-surface cases, respectively. Section 4.3, finally, presents overall pseudo-codes for the complete scattering algorithms.

4.1 Closed-surface case

4.1.1 Surface partitioning and discretization

The proposed numerical method evaluates the necessary weakly-singular operators \mathcal{H} on the basis of the Chebyshev-based rectangular-polar solver developed in [12]. We thus assume the scattering surface has been partitioned into a set of M non-overlapping "logically-quadrilateral" parametrized patches (i.e. patches that can be parametrized from the parameter square $[-1, 1] \times [-1, 1]$), which can easily be obtained, for example, from typical CAD (Computer Aided Design) models. Let, then, the non-overlapping partition of the scattering surface be given by the union of logically-rectangular patches Γ_q ,

$$\Gamma = \bigcup_{q=1}^M \Gamma_q, \quad \Gamma_q := \{x = \mathbf{r}^q(u, v) : [-1, 1]^2 \rightarrow \mathbb{R}^3\}.$$

Then the integral \mathcal{H} over Γ can be decomposed as a sum of integrals over each one of the patches:

$$\mathcal{H}(x) = \sum_{q=1}^M \mathcal{H}_q(x), \quad \mathcal{H}_q(x) := \int_{\Gamma_q} H(x, y)\varphi(y)ds_y, \quad x \in \Gamma.$$

Once the patch structure has been established, a number of “singular”, “near-singular” and “regular” integration problems arise as described in Section 4.2, for which specialized rules are used for accuracy and efficiency. In all cases the numerical method we use incorporates Fejér’s first quadrature rule, which effectively exploits the discrete orthogonality property satisfied by the Chebyshev polynomials in the Chebyshev meshes. Denoting by $\tau_j \in [-1, 1], j = 0, \dots, N-1$ the N Chebyshev points

$$\tau_j = \cos\left(\frac{2j+1}{2N}\pi\right), \quad j = 0, \dots, N-1,$$

Using the Cartesian-product discretization $\{u_i = \tau_i | i = 1, \dots, N\} \times \{v_j = \tau_j | j = 1, \dots, N\}$, we choose the discretization points in each patch Γ_q according to

$$x_{ij}^q = \mathbf{r}^q(u_i, v_j), \quad i, j = 0, \dots, N-1.$$

Then, a given density φ with values $\varphi_{ij}^q = \varphi(x_{ij}^q)$ is approximated by means of the Chebyshev expansion

$$\varphi(x) \approx \sum_{i,j=0}^{N-1} \varphi_{ij}^q a_{ij}(u, v), \quad x \in \Gamma_q,$$

where

$$a_{ij}(u, v) = \frac{1}{N^2} \sum_{m,n=0}^{N-1} \alpha_n \alpha_m T_n(u_i) T_m(v_j) T_n(u) T_m(v), \quad \alpha_n = \begin{cases} 1, & n = 0, \\ 2, & n \neq 0. \end{cases}$$

As is well known the functions $a_{ij}(u, v)$ satisfy the relations

$$a_{ij}(u_n, v_m) = \begin{cases} 1, & (n, m) = (i, j), \\ 0, & \text{otherwise.} \end{cases}$$

4.1.2 Non-adjacent and adjacent integration

The method we use for evaluation of an integral \mathcal{H}_q of the form (4.1) at the discretization points $x_{ij}^{\tilde{q}}$ ($\tilde{q} = 1, \dots, M$) proceeds by consideration of the distance

$$\text{dist}_{x, \Gamma_q} := \min_{(u,v) \in [-1,1]^2} \{|x - \mathbf{r}^q(u, v)|\}$$

between the point x and the patch Γ_q . Denote the index sets

$$\mathbf{I}_a := \{(q, \tilde{q}, i, j) | \text{dist}_{x_{ij}^{\tilde{q}}, \Gamma_q} \leq \tau, q, \tilde{q} = 1, \dots, M, i, j = 1, \dots, N\}, \quad (4.4)$$

$$\mathbf{I}_{na} := \{(q, \tilde{q}, i, j) | \text{dist}_{x_{ij}^{\tilde{q}}, \Gamma_q} > \tau, q, \tilde{q} = 1, \dots, M, i, j = 1, \dots, N\}, \quad (4.5)$$

where τ is some tolerance (in this paper, we use $\tau = 0.1$).

In the "non-adjacent" integration case, in which the point $x_{ij}^{\tilde{q}}$ is far from the integration patch (i.e., $(q, \tilde{q}, i, j) \in \mathbf{I}_{na}$), the integrand $\mathcal{H}_q(x_{ij}^{\tilde{q}})$ is smooth. Then this integral can be accurately evaluated by means of Fejér’s first quadrature rule

$$\begin{aligned} \mathcal{H}_q(x_{ij}^{\tilde{q}}) &= \int_{\Gamma_q} H(x_{ij}^{\tilde{q}}, y) \varphi(y) ds_y \\ &= \int_{-1}^1 \int_{-1}^1 H(x_{ij}^{\tilde{q}}, \mathbf{r}^q(u, v)) \varphi(\mathbf{r}^q(u, v)) J^q(u, v) dudv \\ &\approx \sum_{m,n=0}^{N-1} H(x_{ij}^{\tilde{q}}, \mathbf{r}^q(u_n, v_m)) \varphi_{nm}^q J^q(u_n, v_m) w_n w_m, \end{aligned} \quad (4.6)$$

where $J^q(u, v)$ denotes the surface Jacobian and $w_j, j = 0, \dots, N-1$ are the quadrature weights

$$w_j = \frac{2}{N} \left(1 - 2 \sum_{l=1}^{\lfloor N/2 \rfloor} \frac{1}{4l^2 - 1} \cos(lu_j) \right), \quad j = 0, \dots, N-1.$$

In the "adjacent" integration case, in which the point $x_{ij}^{\tilde{q}}$ either lies within the integration patch or is "close" to it (i.e., $(q, \tilde{q}, i, j) \in \mathbb{I}_a$), in turn, the problem of evaluation of $\mathcal{H}_q(x_{ij}^{\tilde{q}})$ presents a challenge in view of the singularity or nearly-singularity of its kernel. To tackle this difficulty we apply a change of variables whose derivatives vanish at the singularity or, for nearly singular problems, at the point in the integration patch that is closest to the singularity—in either case, the coordinates $(\tilde{u}^q, \tilde{v}^q) \in [-1, 1]$ of the point around which refinements are performed are given by

$$(\tilde{u}^q, \tilde{v}^q) = \arg \min_{(u,v) \in [-1,1]^2} \left\{ |x_{ij}^{\tilde{q}} - \mathbf{r}^q(u, v)| \right\}.$$

The quantities \tilde{u}^q, \tilde{v}^q can be found by means of an appropriate minimization algorithm such as the golden section search algorithm. A "rectangular-polar" change of variables can be constructed on the basis of the one-dimensional change of variables

$$\xi_\alpha(t) = \begin{cases} \alpha + \frac{\text{sgn}(t) - \alpha}{\pi} w_p(\pi|t|), & \alpha \neq \pm 1, \\ \alpha - \frac{1+\alpha}{\pi} w_p\left(\pi \frac{|t-1|}{2}\right), & \alpha = 1, \\ \alpha + \frac{1-\alpha}{\pi} w_p\left(\pi \frac{|t+1|}{2}\right), & \alpha = -1. \end{cases}$$

Here $w_p(t)$ is a function depending on a constant $p \geq 2$ given by

$$w_p(t) = 2\pi \frac{[\eta_p(t)]^p}{[\eta_p(t)]^p + [\eta_p(2\pi - t)]^p}, \quad 0 \leq t \leq 2\pi,$$

where

$$\eta_p(t) = \left(\frac{1}{p} - \frac{1}{2} \right) \left(\frac{\pi - t}{\pi} \right)^3 + \frac{1}{p} \left(\frac{\pi - t}{\pi} \right) + \frac{1}{2}.$$

It is easy to check that the derivatives of $w_p(t)$ up to order $p-1$ vanish at the endpoints. Applying the Chebyshev expansion of the density φ , the above change of variables and the Fejér's first quadrature rule, we obtain

$$\begin{aligned} \mathcal{H}_q(x_{ij}^{\tilde{q}}) &= \int_{\Gamma_q} H(x_{ij}^{\tilde{q}}, y) \varphi(y) ds_y \\ &\approx \sum_{n,m=0}^{N-1} \varphi_{nm}^q \int_{-1}^1 \int_{-1}^1 H(x_{ij}^{\tilde{q}}, \mathbf{r}^q(u, v)) J^q(u, v) a_{nm}(u, v) dudv \\ &= \sum_{n,m=0}^{N-1} \varphi_{nm}^q \int_{-1}^1 \int_{-1}^1 \tilde{H}(x_{ij}^{\tilde{q}}, s, t) \tilde{J}^q(s, t) \tilde{a}_{nm}(s, t) \xi_{\tilde{u}^q}^l(s) \xi_{\tilde{v}^q}^l(t) ds dt \\ &\approx \sum_{n,m=0}^{N-1} A_{ij, nm}^{\tilde{q}, q} \varphi_{nm}^q \end{aligned} \tag{4.7}$$

where

$$A_{ij, nm}^{\tilde{q}, q} = \sum_{l_1, l_2}^{N^\beta - 1} \tilde{H}(x_{ij}^{\tilde{q}}, \tilde{u}_{l_1}, \tilde{u}_{l_2}) \tilde{J}^q(\tilde{u}_{l_1}, \tilde{u}_{l_2}) \tilde{a}_{nm}(\tilde{u}_{l_1}, \tilde{u}_{l_2}) \xi_{\tilde{u}^q}^l(\tilde{u}_{l_1}) \xi_{\tilde{v}^q}^l(\tilde{u}_{l_2}) \tilde{w}_{l_1} \tilde{w}_{l_2}, \tag{4.8}$$

with

$$\begin{aligned}\tilde{H}(x_{ij}^q, s, t) &= H(x_{ij}^q, \mathbf{r}^q(\xi_{\tilde{u}^q}(s), \xi_{\tilde{v}^q}(t))), \\ \tilde{J}^q(s, t) &= J^q(\xi_{\tilde{u}^q}(s), \xi_{\tilde{v}^q}(t)), \\ \tilde{a}_{nm}(s, t) &= a_{nm}(\xi_{\tilde{u}^q}(s), \xi_{\tilde{v}^q}(t)),\end{aligned}$$

and where the quadrature nodes and weights are given by

$$\tilde{u}_j = \cos\left(\frac{2j+1}{2N^\beta}\pi\right), \quad j = 0, \dots, N^\beta - 1,$$

and

$$\tilde{w}_j = \frac{2}{N^\beta} \left(1 - 2 \sum_{l=1}^{\lfloor N^\beta/2 \rfloor} \frac{1}{4l^2 - 1} \cos(l\tilde{u}_j) \right), \quad j = 0, \dots, N^\beta - 1.$$

Using sufficiently large numbers N^β of discretization points along the u and v directions to accurately resolve the challenging integrands, all singular and nearly singular problems can be treated with high accuracy under discretizations that are not excessively fine.

4.1.3 Evaluation of surface gradients

Now we describe the implementation we use for the evaluation of the surface gradient ∇^S , from which the needed surface-differentiation operators $M(\partial, \nu)$, $\mathcal{T}_1, \mathcal{T}_2$ can be extracted. On each patch Γ_q , the surface gradient of a given density $\psi(u, v) = \varphi(\mathbf{r}^q(u, v))$ is given by

$$\nabla_x^S \psi = g^{11} \frac{d\psi}{du} \frac{d\mathbf{r}^q}{du} + g^{12} \frac{d\psi}{du} \frac{d\mathbf{r}^q}{dv} + g^{21} \frac{d\psi}{dv} \frac{d\mathbf{r}^q}{du} + g^{22} \frac{d\psi}{dv} \frac{d\mathbf{r}^q}{dv},$$

where g^{ij} , $i, j = 1, 2$ denote the components of the inverse of the first fundamental matrix $G = [g_{ij}]_{i,j=1}^2$ with

$$\begin{aligned}g_{11} &= \frac{d\mathbf{r}^q}{du} \cdot \frac{d\mathbf{r}^q}{du}, & g_{12} &= \frac{d\mathbf{r}^q}{du} \cdot \frac{d\mathbf{r}^q}{dv}, \\ g_{21} &= \frac{d\mathbf{r}^q}{dv} \cdot \frac{d\mathbf{r}^q}{du}, & g_{22} &= \frac{d\mathbf{r}^q}{dv} \cdot \frac{d\mathbf{r}^q}{dv}.\end{aligned}$$

The quantities $\frac{d\psi}{du}$, $\frac{d\psi}{dv}$ can be easily evaluated by means of term-by-term differentiation of the Chebyshev expansion of ψ . Therefore, we have

$$(\nabla_x^S \psi) \Big|_{x=x_{ij}^q} = \sum_{n,m=0}^{N-1} B_{ij, nm}^q \varphi_{nm}^q,$$

where

$$B_{ij, nm}^q = \left(g^{11} \frac{da_{nm}}{du} \frac{d\mathbf{r}^q}{du} + g^{12} \frac{da_{nm}}{du} \frac{d\mathbf{r}^q}{dv} + g^{21} \frac{da_{nm}}{dv} \frac{d\mathbf{r}^q}{du} + g^{22} \frac{da_{nm}}{dv} \frac{d\mathbf{r}^q}{dv} \right) \Big|_{u=u_i, v=v_j}. \quad (4.9)$$

4.2 Open-surface case

4.2.1 Surface partitioning, discretization and integration

As we did for closed surfaces, here we assume the open scattering surface has been partitioned into a set of M non-overlapping logically-rectangular patches Γ_q ,

$$\Gamma = \bigcup_{q=1}^M \Gamma_q, \quad \Gamma_q := \{x = \hat{\mathbf{r}}^q(u, v) : [-1, 1]^2 \rightarrow \mathbb{R}^3\}.$$

Then the integrals $\widehat{\mathcal{H}}^1$ and $\widehat{\mathcal{H}}^2$ can be decomposed as sums of integrals over each one of the patches:

$$\widehat{\mathcal{H}}^1(x) = \sum_{q=1}^M \widehat{\mathcal{H}}_q^1(x), \quad \widehat{\mathcal{H}}_q^1(x) := \int_{\Gamma_q} H(x, y) \varphi(y) w(y) ds_y, \quad x \in \Gamma, \quad (4.10)$$

$$\widehat{\mathcal{H}}^2(x) = \sum_{q=1}^M \widehat{\mathcal{H}}_q^2(x), \quad \widehat{\mathcal{H}}_q^2(x) := \int_{\Gamma_q} H(x, y) \varphi(y) / w(y) ds_y, \quad x \in \Gamma. \quad (4.11)$$

In view of the weight function $w \sim d^{1/2}$ that is present in the integrands of both (4.10) and (4.11), a direct application in the present context of the integration method proposed in Section 4.1.2 only yields accuracy of low order. To demonstrate this fact we consider the integrals

$$I_1 = \int_{-1}^1 \cos(t) \sqrt{1-t^2} dt, \quad I_2 = \int_{-1}^1 \frac{\cos(t)}{\sqrt{1-t^2}} dt,$$

where the term $w(t) = \sqrt{1-t^2}$ is the singular weight function in this case. As demonstrated in Table 1, applications of the Fejer's first quadrature rule to the integrals I_1 and I_2 only yield third- and first-order convergence, respectively.

Table 1: Errors in the evaluation of the integrals I_1 and I_2 by means of Fejer's first quadrature rule.

N	I_1	Order	I_2	Order
5	9.06E-4	–	3.27E-2	–
10	1.65E-4	2.46	1.55E-2	1.08
15	4.87E-5	3.01	1.04E-2	0.98
20	2.12E-5	2.89	7.75E-3	1.02
30	6.30E-6	2.99	5.17E-3	1.00

To evaluate of the integrals (4.10) and (4.11) with high accuracy order we introduce the change of variables

$$u = \eta_u^q(s) = \begin{cases} s, & \text{No edge on } u, \\ \cos(\frac{\pi}{2}(1-s)), & \text{Edges at } u = \pm 1, \\ 1 - 2 \cos(\frac{\pi}{4}(1+s)), & \text{Edge at } u = -1 \text{ only,} \\ 2 \cos(\frac{\pi}{4}(1-s)) - 1, & \text{Edge at } u = 1 \text{ only,} \end{cases}$$

which maps the interval $[-1, 1]$ to itself. Incorporating this change of variables we obtain

$$\widehat{\mathcal{H}}_q^1(x) = \int_{-1}^1 \int_{-1}^1 H(x, \widehat{\mathbf{r}}^q(\eta_u^q(s), \eta_v^q(t))) \varphi(\widehat{\mathbf{r}}^q(\eta_u^q(s), \eta_v^q(t))) \widehat{J}^q(\eta_u^q(s), \eta_v^q(t)) \widetilde{w}_1(s, t) ds dt, \quad (4.12)$$

and

$$\widehat{\mathcal{H}}_q^2(x) = \int_{-1}^1 \int_{-1}^1 H(x, \widehat{\mathbf{r}}^q(\eta_u^q(s), \eta_v^q(t))) \varphi(\widehat{\mathbf{r}}^q(\eta_u^q(s), \eta_v^q(t))) \widehat{J}^q(\eta_u^q(s), \eta_v^q(t)) \widetilde{w}_2(s, t) ds dt, \quad (4.13)$$

where

$$\begin{aligned} w_1(s, t) &= \frac{d\eta_u^q(s)}{ds} \frac{d\eta_v^q(t)}{dt} w(\widehat{\mathbf{r}}^q(\eta_u^q(s), \eta_v^q(t))), \\ w_2(s, t) &= \frac{d\eta_u^q(s)}{ds} \frac{d\eta_v^q(t)}{dt} [w(\widehat{\mathbf{r}}^q(\eta_u^q(s), \eta_v^q(t)))]^{-1}, \end{aligned}$$

and $\widehat{J}^q(\eta_u^q(s), \eta_v^q(t))$ denotes the surface Jacobian. It is easily checked that the integrands in (4.10) and (4.11) equal the products of the weakly singular kernel $H(x, \widehat{\mathbf{r}}^q(\eta_u^q(s), \eta_v^q(t)))$ multiplied by a smooth function.

Using the Cartesian-product discretization $\{s_i = \tau_i | i = 1, \dots, N\} \times \{t_j = \tau_j | j = 1, \dots, N\}$, we choose the discretization points in each patch Γ_q according to

$$\widehat{x}_{ij}^q = \widehat{\mathbf{r}}^q(\eta_u^q(s_i), \eta_v^q(t_j)), \quad i, j = 0, \dots, N-1.$$

Then, a given density φ with values $\widehat{\varphi}_{ij}^q = \varphi(\widehat{x}_{ij}^q)$ is approximated by means of the Chebyshev expansion

$$\varphi(x) \approx \sum_{i,j=0}^{N-1} \widehat{\varphi}_{ij}^q a_{ij}(s, t), \quad x = \widehat{\mathbf{r}}^q(\eta_u^q(s), \eta_v^q(t)) \in \Gamma_q,$$

and the non-adjacent and adjacent evaluation of the integrals (4.12) and (4.13) with respect to (s, t) at the discretization points \widehat{x}_{ij}^q , $q = 1, \dots, M$, $i, j = 1, \dots, N$ is then produced, with high-order accuracy, by means of the numerical strategy presented in Section 4.1.2.

4.2.2 Evaluation of surface gradients

Finally, we describe the implementation we use for the evaluation of the surface gradient ∇^S and associated operators $M(\partial, \nu)$, \mathcal{T}^w and \mathcal{T}_1^w for open-surface problems. Incorporating the open-surface change of variables introduced in Section 4.2.1, the surface gradient of a given density $\psi(s, t) = \varphi(\mathbf{r}^q(\eta_u^q(s), \eta_v^q(t)))$ on each patch Γ_q is given by

$$\nabla_x^S \psi = \widehat{g}^{11} \frac{d\psi}{ds} \frac{d\mathbf{r}^q}{du} \frac{d\eta_u^q(s)}{ds} + \widehat{g}^{12} \frac{d\psi}{ds} \frac{d\mathbf{r}^q}{dv} \frac{d\eta_v^q(t)}{dt} + \widehat{g}^{21} \frac{d\psi}{dt} \frac{d\mathbf{r}^q}{du} \frac{d\eta_u^q(s)}{ds} + \widehat{g}^{22} \frac{d\psi}{dt} \frac{d\mathbf{r}^q}{dv} \frac{d\eta_v^q(t)}{dt},$$

where \widehat{g}^{ij} , $i, j = 1, 2$ denote the components of the inverse of the first fundamental matrix $\widehat{G} = [\widehat{g}_{ij}]_{i,j=1}^2$ with

$$\begin{aligned} \widehat{g}_{11} &= \frac{d\eta_u^q(s)}{ds} \frac{d\eta_u^q(s)}{ds} \left(\frac{d\mathbf{r}^q}{du} \cdot \frac{d\mathbf{r}^q}{du} \right), & \widehat{g}_{12} &= \frac{d\eta_u^q(s)}{ds} \frac{d\eta_v^q(t)}{dt} \left(\frac{d\mathbf{r}^q}{du} \cdot \frac{d\mathbf{r}^q}{dv} \right), \\ \widehat{g}_{21} &= \frac{d\eta_u^q(s)}{ds} \frac{d\eta_v^q(t)}{dt} \left(\frac{d\mathbf{r}^q}{dv} \cdot \frac{d\mathbf{r}^q}{du} \right), & \widehat{g}_{22} &= \frac{d\eta_v^q(t)}{dt} \frac{d\eta_v^q(t)}{dt} \left(\frac{d\mathbf{r}^q}{dv} \cdot \frac{d\mathbf{r}^q}{dv} \right). \end{aligned}$$

Analogously, the quantities $\frac{d\psi}{ds}$, $\frac{d\psi}{dt}$ can be easily evaluated by means of term-by-term differentiation of the Chebyshev expansion of ψ . Therefore, we have

$$(\nabla_x^S \psi) \Big|_{x=\widehat{x}_{ij}^q} = \sum_{n,m=0}^{N-1} \widehat{B}_{ij,nm}^q \varphi_{nm}^q,$$

where

$$\begin{aligned} \widehat{B}_{ij,nm}^q &= \left(\widehat{g}^{11} \frac{da_{nm}}{ds} \frac{d\mathbf{r}^q}{du} \frac{d\eta_u^q(s)}{ds} + \widehat{g}^{12} \frac{da_{nm}}{ds} \frac{d\mathbf{r}^q}{dv} \frac{d\eta_v^q(t)}{dt} \right. \\ &\quad \left. + \widehat{g}^{21} \frac{da_{nm}}{dt} \frac{d\mathbf{r}^q}{du} \frac{d\eta_u^q(s)}{ds} + \widehat{g}^{22} \frac{da_{nm}}{dt} \frac{d\mathbf{r}^q}{dv} \frac{d\eta_v^q(t)}{dt} \right) \Big|_{s=s_i, t=t_j}. \end{aligned}$$

4.3 Overall algorithm pseudocode

Utilizing the concepts presented in Section 4.1, the proposed algorithm for solution of problems of elastic scattering by closed surfaces is summarized in the following pseudocode. Relying on Section 4.2 instead of 4.1, the corresponding pseudocode for open-surface problems is completely analogous, and is therefore omitted.

I. Initialization. Input values of M, N, N^β, τ, p and construct the surface partitioning and discretization points $x_{ij}^q, q = 1, \dots, M, i, j = 1, \dots, N$;

II. Precomputation.

- i. For all $\tilde{q}, q = 1, \dots, M, i, j = 1, \dots, N$, compute the index sets I_a and I_{na} , see (4.4) and (4.5);
- ii. Compute the matrices $A_{ij, nm}^{\tilde{q}}, (q, \tilde{q}, i, j) \in I_a, n, m = 1, \dots, N$ given in (4.8) for adjacent integration;
- iii. Compute the matrices $B_{ij, nm}^q, q = 1, \dots, M, i, j, n, m = 1, \dots, N$ given in (4.9) for evaluation of surface gradients;

III. Iterative solution. Use the iterative solver GMRES to approximate the solution of the discrete form of the linear equation (2.9) or (3.4). The necessary matrix-vector products are obtained by suitable compositions and combinations, as detailed in Sections 4.1.2 and 4.1.3, of the matrices obtained per point II above.

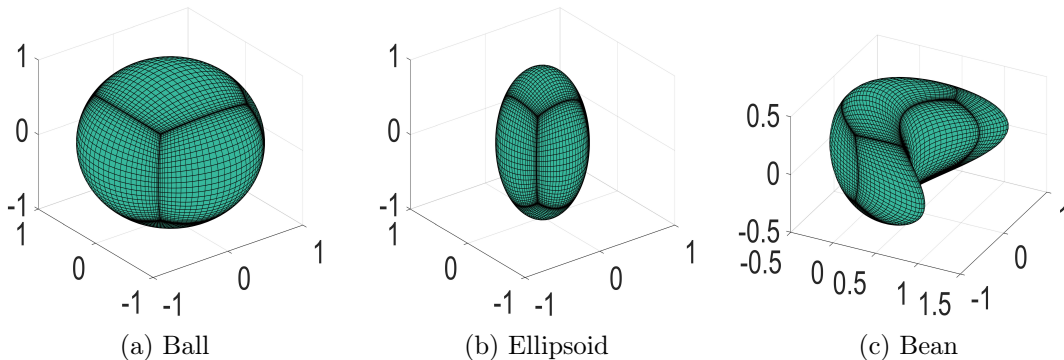


Figure 4: Obstacles used in the numerical tests presented in Section 5.

5 Numerical experiments

This section presents a variety of numerical tests that demonstrate the accuracy and efficiency of the proposed three-dimensional elastic scattering solver—or, more precisely, the accuracy and efficiency of the computational implementations presented in Section 4 for the regularized integral equations (3.4) and (3.7) and associated field evaluation expressions. For definiteness, the Lamé constants and densities for the elastic medium are assumed as follows: $\lambda = 2, \mu = 1, \rho = 1$. Solutions for the integral equations were produced by means of the fully complex version of the iterative solver GMRES with residual tolerance ϵ_r as specified in each case. The maximum errors presented in this section are calculated in accordance with the expression

$$\epsilon_\infty := \frac{\max_{x \in S} \{|u^{\text{num}}(x) - u^{\text{ref}}(x)|\}}{\max_{x \in S} \{|u^{\text{ref}}(x)|\}},$$

where S is the square $[-1, 1] \times [-1, 1] \times \{2\} \subset D$, and where u^{ref} is produced, for each example, through evaluation of exact solutions u^{ex} when available, or by means of numerical solution with sufficiently fine discretizations, otherwise. All of the numerical tests were obtained by means of Fortran numerical implementations, parallelized using OpenMP, on a single node (twenty-four computing cores) of a dual socket Dell R420 with two Intel Xenon E5-2670 v3 2.3 GHz, 128GB of RAM.

In our first experiment we evaluate the accuracy of the discretization methods used for the operators \mathcal{T}_1 and \mathcal{T}_2 on a sphere partitioned as indicated in Figure 4(a), and using the scalar and vector functions

$$v(x) = \sin(x_1)e^{i(x_2+x_3)}, \quad V(x) = (\sin(x_1), \cos(x_2), e^{ix_3}).$$

As indicated in Section 4.3, the functions \mathcal{T}_1v and \mathcal{T}_2V are evaluated in our context via term-by-term differentiation of the Chebyshev expansions of v and V . The resulting differentiation errors, evaluated as a maximum over all discretization points, are presented in Table 2—which, in particular, displays the expected exponential convergence.

Table 2: Errors in the evaluation of the operators \mathcal{T}_1 and \mathcal{T}_2 .

N	\mathcal{T}_1v	\mathcal{T}_2V
5	1.03E-1	1.83E-2
10	3.22E-4	6.36E-5
15	1.29E-6	7.41E-8
20	1.82E-9	9.96E-11
25	3.16E-12	2.11E-12

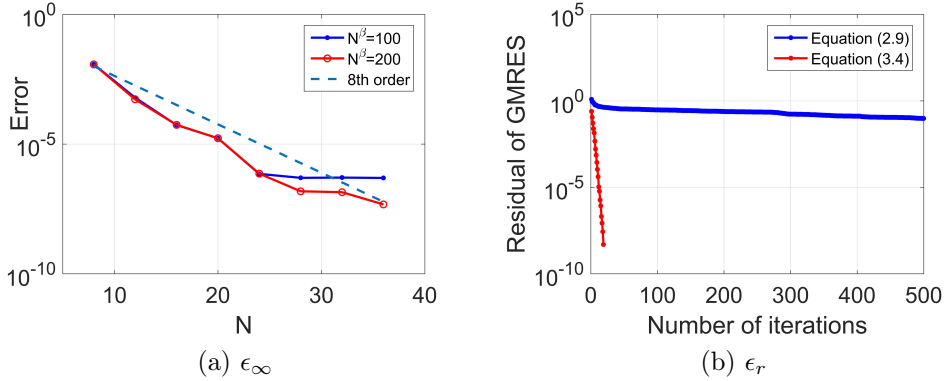


Figure 5: Numerical errors (a) and GMRES residual (b) for the problem of scattering by the spherical obstacle.

Next, we demonstrate the high accuracy and rapid convergence of the proposed closed-surface elastic scattering method via applications to the three bounded obstacles depicted in Figure 4. In each case boundary conditions were used for which the exact solution is given by an pressure point source located at a point z within the ball:

$$u^{\text{ex}}(x) = \frac{1}{k_p} \nabla_x \frac{e^{ik_p|x-z|}}{4\pi|x-z|}.$$

(While not physically motivated, this exact solution and associated boundary conditions provide a commonly used test for evaluation of the accuracy of the scattering solver.) The source was assumed to be located at $z = (0, 0.5, 0.3)$ for the spherical scatterer, and at $z = (0, 0, 0)$ for the ellipsoidal and bean-shaped obstacles. Figures 5(a), 6(a) and 7(a) display the errors in the numerical solution for the frequency $\omega = 2\pi$, produced by means of the regularized integral equation (3.4), as a function of N . In all three cases $M = 6$ patches were used, together with two different values of the rectangular-integration parameter, namely $N^\beta = 100$ and $N^\beta = 200$. These figures clearly demonstrate the fast convergence and high accuracy of the algorithm. Figures 5(b), 6(b) and 7(b), in turn, display the GMRES residuals as functions of the number of iterations, in the numerical solution of the un-regularized (resp. regularized)

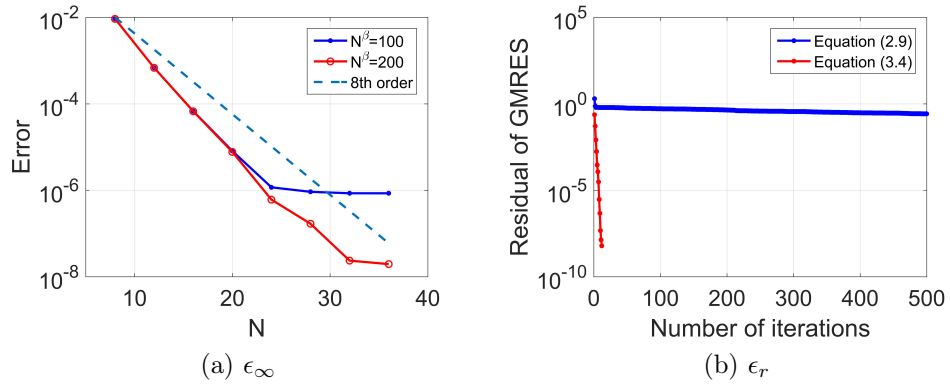


Figure 6: Numerical errors (a) and GMRES residual (b) for the problem of scattering by the ellipsoidal obstacle.

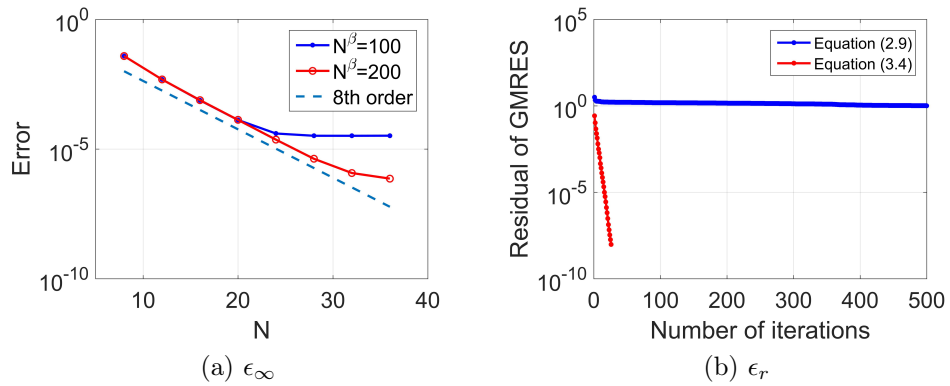


Figure 7: Numerical errors (a) and GMRES residual (b) for the problem of scattering by the bean-shaped obstacle.

integral equation (2.9) (resp. (3.4)), for which we used $N = 36$ and $N^\beta = 200$. Clearly, use of the regularized equation is highly beneficial: using only 19, 12 and 28 iterations the solver achieves the GMRES tolerance $\epsilon_r = 1 \times 10^{-8}$ for the spherical, ellipsoidal and bean-shaped obstacles, respectively. This is in striking contrast with the numbers of iterations required by the implementation based on the unregularized equation, which are also displayed in these figures. Table 3 presents the numerical solution errors together with other statistics such as precomputation time, time per iteration and number of iterations used for a problem of scattering at frequency $\omega = 10\pi$ on the basis of six 5×5 patches. At this frequency, $N = 8$ (resp. $N = 16$) suffices to produce an accuracy 4.67×10^{-3} (resp. 1.39×10^{-6}).

Table 3: Numerical errors in the numerical total field for the problem of scattering by a sphere of diameter $10\lambda_s$ produced by the solver based on the regularized equation (3.4).

N	N^β	N_{DOF}	Time (prec.)	Time (1 iter.)	$N_{\text{iter}} (\epsilon_r)$	ϵ_∞
8	50	$3 \times 9,600$	11.63 s	8.32 s	22 (9.41×10^{-4})	4.77×10^{-3}
8	100	$3 \times 9,600$	43.22 s	8.32 s	21 (9.88×10^{-4})	4.67×10^{-3}
16	50	$3 \times 38,400$	1.09 min	2.14 min	32 (1.05×10^{-5})	1.32×10^{-4}
16	100	$3 \times 38,400$	3.52 min	2.16 min	34 (9.73×10^{-7})	1.39×10^{-6}

We next consider the plane-wave incident pressure field

$$u^{inc} = de^{ik_p x \cdot d}, \quad d = (\sin \theta_1 \cos \theta_2, \sin \theta_1 \sin \theta_2, \cos \theta_1), \quad (5.1)$$

where (θ_1, θ_2) denote the polar and azimuthal incidence angles. For our example we use the two pairs of angles $\theta_1 = \pi/2, \theta_2 = 0$ and $\theta_1 = \pi, \theta_2 = 0$ for the spherical, and bean-shaped obstacles, respectively, and we take $\omega = 10\pi$, $M = 6 \times 5 \times 5 = 150$ patches (the six original patches subdivided into 5×5 each), and $N = 16$ (for a total number $N_{\text{DOF}} = 115200$ of degrees of freedom in the problem). Figures 8 and 9 display the resulting numerical solutions.

Finally, we consider the problem of elastic scattering by a unit disc

$$x^2 + y^2 \leq 1, \quad z = 0,$$

for which the weight function $w = \sqrt{1 - x^2 - y^2}$ was used, under plane pressure incidence field (5.1) with incidence angles $\theta_1 = \pi$ and $\theta_2 = 0$. This problem can be tackled by means of either the first-kind equation (2.13) or the regularized equation (3.7). Figure 10 displays the errors in the numerical solution as a function of N , demonstrating once again fast convergence and high accuracy. The values $M = 5$ and $N^\beta = 200$ were used. Figures 11 and 12 present the GMRES residuals as a function of the number of iterations for the various formulations (2.13), (3.7), (3.8) and (3.9). Clearly, the Neumann solver based on the regularized integral equation (3.7) requires a significantly smaller number of GMRES iterations, to meet a given GMRES tolerance ϵ_r , than the corresponding solver based on equation (2.13). But for the Dirichlet problem, the regularized equation (3.9) does not provide an improvement over equation (3.8): it actually requires a slightly larger number of iterations in this case. The total computing cost of the regularized equation (3.9) is higher than (3.8) in this case, since the application of the operator S_w is significantly less expensive than the application of operator $N_w S_w$ —and, thus, use of the formulation based on the unregularized operator S_w is recommended for the Dirichlet case. It is worth noting that, in absolute computing times, the cost of evaluation of each open-surface operator N_w and S_w is comparable, for a given overall number of discretization points, to the cost required by the corresponding closed-surface operators N and S , respectively; cf. e.g. Figure 10. Figures 13 and 14 display the total field scattered under the Neumann and Dirichlet problem, respectively. In Figure 13 the famous Poisson spot is clearly visible at the center of the shadow area of the third component of the field.

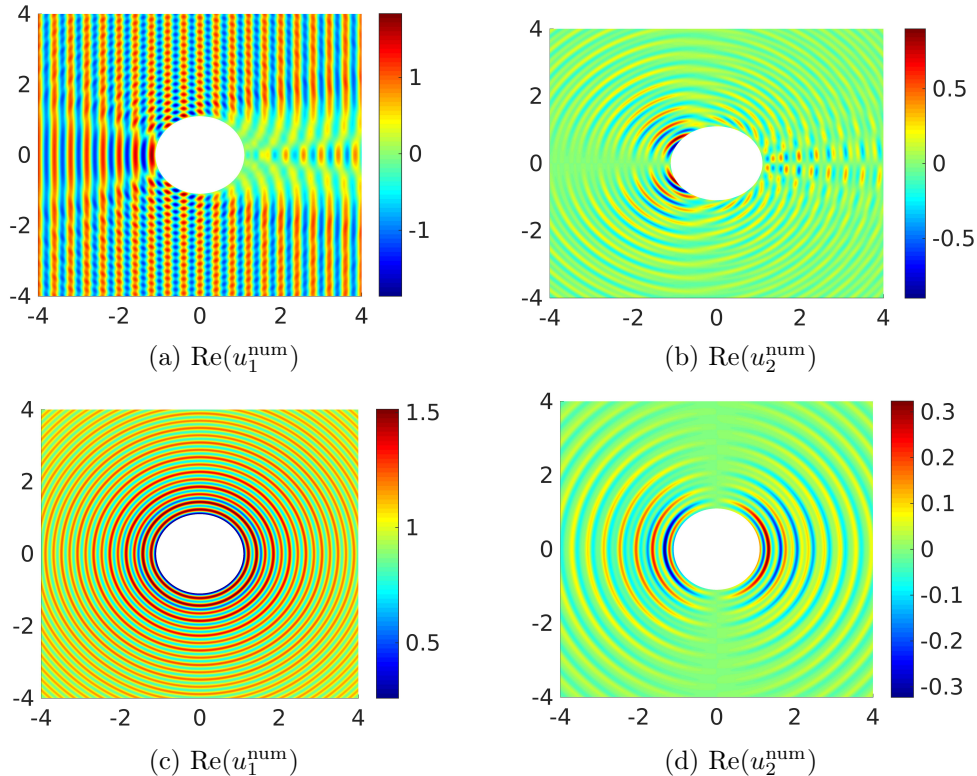


Figure 8: Real parts of the components u_1 and u_2 of the total field u on an $x_3 = 0$ section (Figs. (a) and (b)) and an $x_1 = 0$ section (Figs. (c) and (d)) for the scattering of a plane-wave pressure incident field, with incidence angles $\theta_1 = \pi/2$, $\theta_2 = 0$, by the spherical obstacle. A total of forty-seven iterations sufficed in this case for the solver to reach the GMRES residual tolerance value $\epsilon_r = 1 \times 10^{-4}$.

6 Conclusions

This paper introduced novel regularized integral formulations and associated fast high-order algorithms for the solution of 3D elastic scattering problems with Neumann and Dirichlet boundary conditions on closed and open surfaces. It was shown that the rectangular integration method [12] and associated Chebyshev differentiation strategies reliably provide high-order accuracies for the weakly singular, strongly singular and hypersingular operators associated with the closed- and open-surface formulations considered. Relying on the newly studied Calderón formulation for 3D elastic waves, the new integral operators inherent in the regularized integral formulations enjoy excellent spectral properties and can give rise to significantly reduced GMRES iterations numbers for a given GMRES tolerance. For the problems with Dirichlet boundary conditions on open surfaces, in turn, application of the weighted single-layer operator is preferable. The regularized integral equation methods for other scattering problems (for example, elastic transmission problems, thermo- and porous-elastic problems, open-surface electromagnetic problems) are left for future work.

References

- [1] C. Alves, R. Kress, On the far-field operator in elastic obstacle scattering, *IMA J. Appl. Math.* 67 (2002) 1-21.

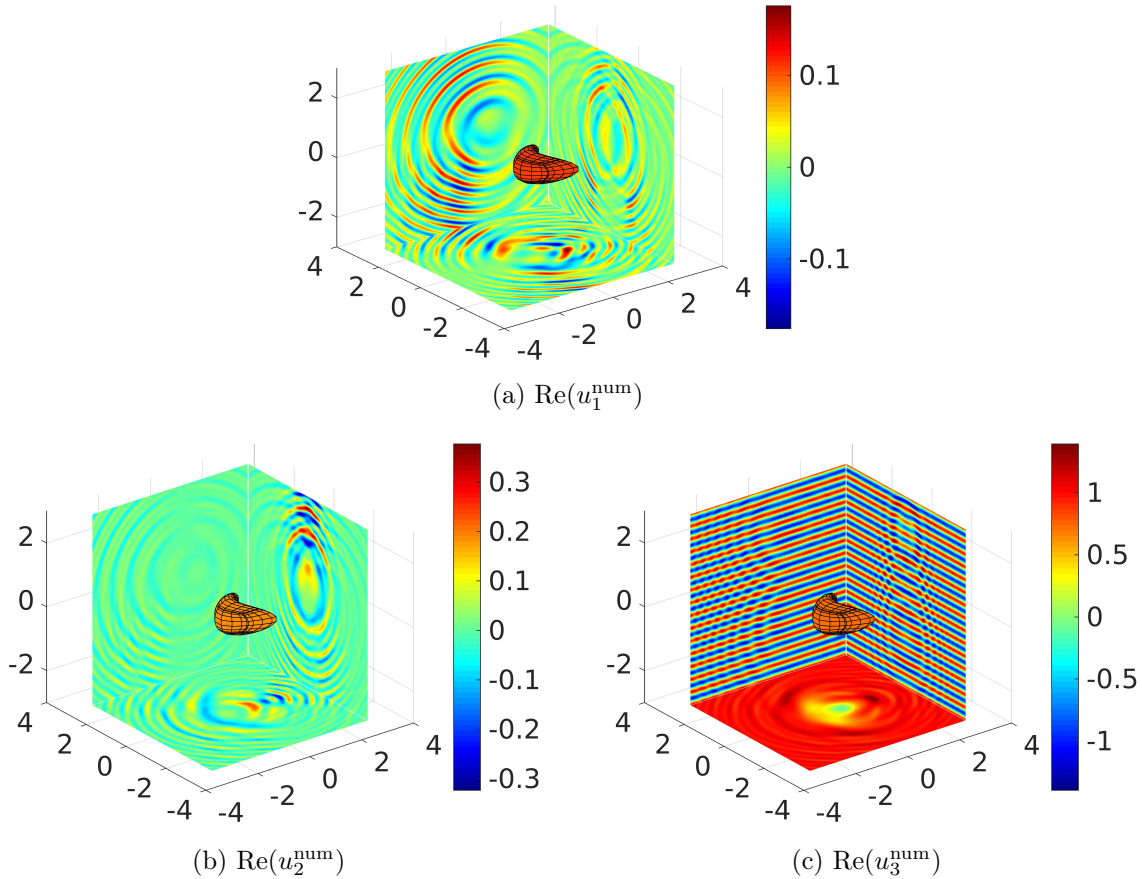


Figure 9: Scattering of a plane-wave pressure incident field with incident angles $\theta_1 = \pi$ and $\theta_2 = 0$ by the bean-shaped obstacle. Total field. The solver required eighty-one iterations to reach the GMRES tolerance value $\epsilon_r = 1 \times 10^{-4}$.

- [2] C. Alves, T.H. Duong, Numerical resolution of the boundary integral equations for elastic scattering by a plane crack, *Int. J. Numer. Meth. Eng.* 38 (1995) 2347-2371.
- [3] K. Ando, Y. Ji, H. Kang, K. Kim, S. Yu, Spectral properties of the Neumann-Poincaré operator and cloaking by anomalous localized resonance for the elasto-static system, *Euro. J. Appl. Math* 29 (2018) 189-225.
- [4] K. Ando, H. Kang, Y. Miyanishi, Elastic Neumann-Poincaré operators on three dimensional smooth domains: Polynomial compactness and spectral structure, *Int. Math. Res. Notices* 2019(12) (2019) 3883-3900.
- [5] X. Antoine, M. Darbas, Alternative integral equations for the iterative solution of acoustic scattering problems. *Quarterly J. Mech. Appl. Math.* 58(1) (2005) 107-128.
- [6] X. Antoine, M. Darbas, Generalized combined field integral equations for the iterative solution of the three-dimensional Helmholtz equation, In *Mathematical modeling and numerical analysis* 41 (2007) 147-167.
- [7] G. Bao, G. Hu, J. Sun, T. Yin, Direct and inverse elastic scattering from anisotropic media, *J. Math. Pures Appl.* 117 (2018) 263-301.

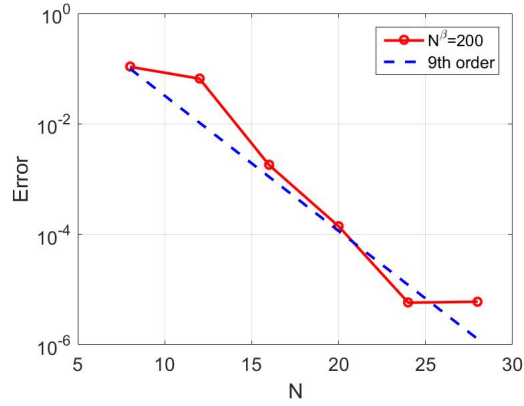


Figure 10: Numerical errors for the problem of scattering by a unit disc of diameter $2\lambda_s$. The accuracy limitation at a level of approximately 10^{-5} corresponds to the choice $N^\beta = 200$; higher accuracies can be obtained by using suitably larger values of this precomputation-related parameter.

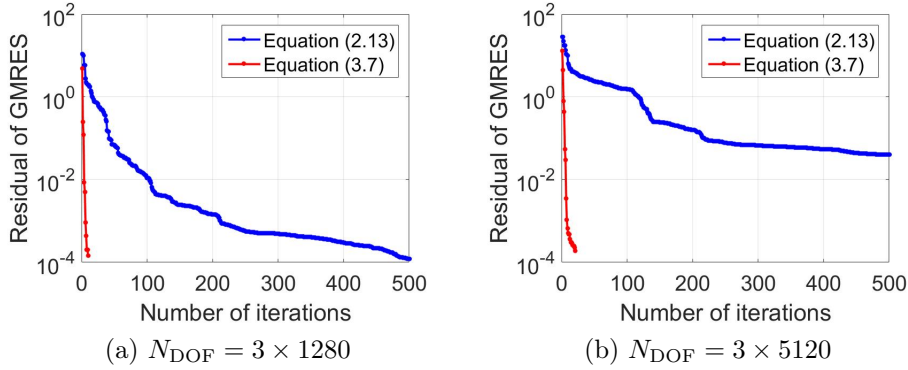


Figure 11: GMRES residuals obtained in the solution of the Neumann problem of scattering by a unit disc with diameter (a) $2\lambda_s$ and (b) $4\lambda_s$.

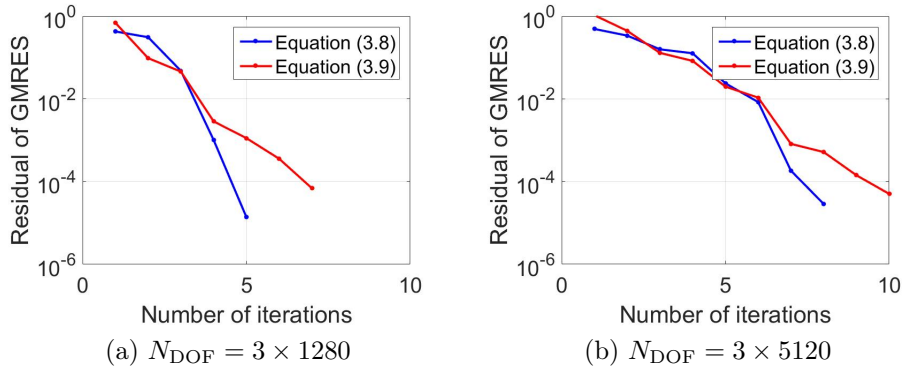


Figure 12: GMRES residuals obtained in the solution of the Dirichlet problem of scattering by a unit disc with diameter (a) $2\lambda_s$ and (b) $4\lambda_s$.

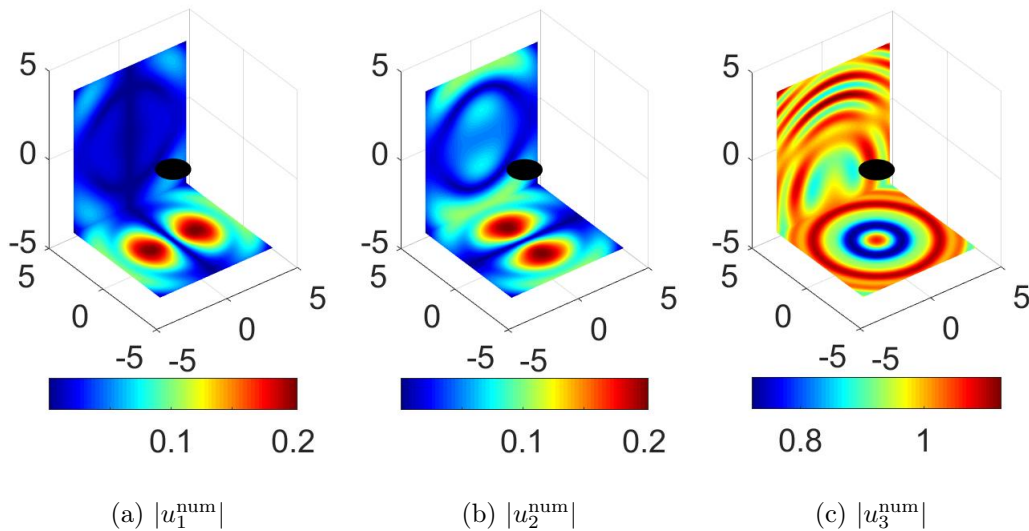


Figure 13: Scattering of a plane-wave pressure incident wave by a unit disc of diameter $2\lambda_s$. Total field under Neumann boundary conditions.

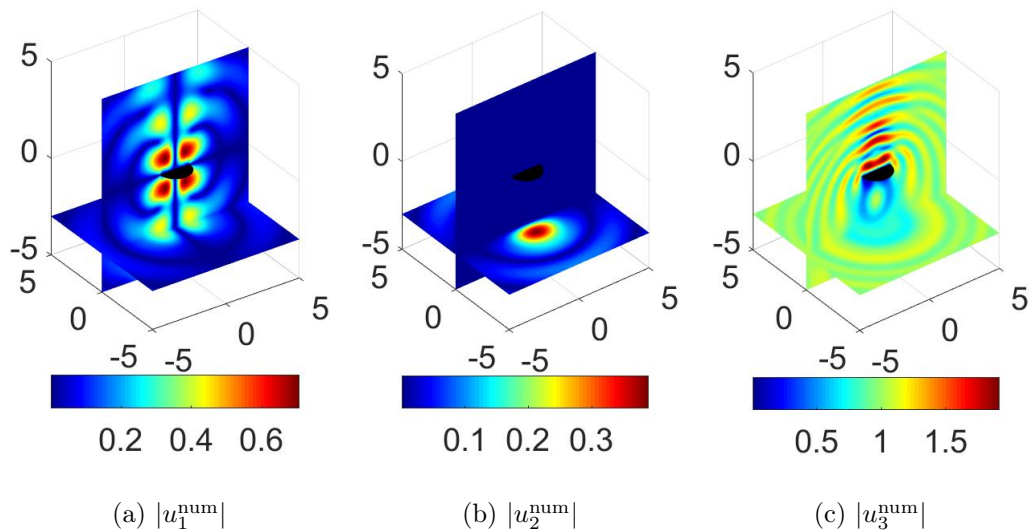


Figure 14: Scattering of a plane-wave pressure incident wave by a unit disc of diameter $2\lambda_s$. Total field under Dirichlet boundary conditions.

- [8] G. Bao, L. Xu, T. Yin, An accurate boundary element method for the exterior elastic scattering problem in two dimensions, *J. Comput. Phys.* 348 (2017) 343-363.
- [9] G. Bao, L. Xu, T. Yin, Boundary integral equation methods for the elastic and thermoelastic waves in three dimensions, *Comput. Method Appl. Methanics Eng.* 354 (2019) 464-486.
- [10] M. Benzi, M. Tuma, A sparse approximate inverse preconditioner for nonsymmetric linear systems, *SIAM J. Sci. Comput.* 3(19) (1998) 968-994.
- [11] O.P. Bruno, T. Elling, C. Turc, Regularized integral equations and fast high-order solvers for sound-hard acoustic scattering problems, *Int. J. Numer. Meth. Eng.* 91 (2012) 1045-1072.
- [12] O.P. Bruno, E. Garza, A Chebyshev-based rectangular-polar integral solver for scattering by general geometries described by non-overlapping patches, available at arXiv:1807.01813.
- [13] O.P. Bruno, S. Lintner, Second-kind integral solvers for TE and TM problems of diffraction by open arcs, *Radio Sci.* 47 (6) (2012).
- [14] O.P. Bruno, S. Lintner, A high-order integral solver for scalar problems of diffraction by screens and apertures in three-dimensional space, *J. Comput. Phys.* 252 (2013) 250-274.
- [15] O.P. Bruno, L. Kunyansky, A fast, high-order algorithm for the solution of surface scattering problems: Basic implementation, tests, and applications, *J. Comput. Phys.* 169 (1) (2001) 80-110.
- [16] O.P. Bruno, L. Xu, T. Yin, Weighted integral solvers for elastic scattering by open arcs in two dimensions, available at arxiv:1902.08687.
- [17] F. Bu, J. Lin, F. Reitich, A fast and high-order method for the three-dimensional elastic wave scattering problem, *J. Comput. Phys.* 258 (2014) 856-870.
- [18] B. Carpentieri, I. Duff, L. Giraud, G. Sylvand, Combining fast multipoles techniques and an approximate inverse preconditioner for large electromagnetism calculations, *SIAM J. Sci. Comput.* 27(3) (2005) 774-792.
- [19] S. Chaillat, M. Bonnet, J.-F. Semblat, A multi-level fast multipole BEM for 3-d elastodynamics in the frequency domain, *Comput. Methods Appl. Mech. Eng.* 197 (2008) 4233-4249.
- [20] R. Chapko, R. Kress, L. Monch, on the numerical solution of a hypersingular integral equation for elastic scattering from a planar crack, *IMA J. Numer. Anal.* 20(4) (2000) 345-360.
- [21] D. Colton and R. Kress, *Inverse Acoustic and Electromagnetic Scattering Theory*, Berlin, Springer, 1998.
- [22] M. Costabel, M. Dauge, R. Duduchava, Asymptotics without logarithmic terms for crack problems, *Commun. Partial Differ. Equ.* 28 (2003) 869-926.
- [23] M. Darbas, F. Le Louër, Well-conditioned boundary integral formulations for high-frequency elastic scattering problems in three dimensions, *Math. Meth. Appl. Sci.* 38 (2015) 1705-1733.
- [24] J. Giroire, J. C. Nédélec, Numerical solution of an exterior Neumann problem using a double layer potential, *Math. Comp.* 32 (1978) 973-990.
- [25] M. E. Gurtin, *The Linear Theory of Elasticity*, Handbuch der Physik v. VIa/2, Springer-Verlag, New York-Heidelberg-Berlin, 1972.
- [26] G. C. Hsiao, W. L. Wendland, *Boundary Integral Equations*, Applied Mathematical Sciences, Vol. 164, Springer-verlag, 2008.

- [27] V. D. Kupradze, T. G. Gegelia, M. O. Basheleishvili, T. V. Burchuladze, *Three-Dimensional Problems of the Mathematical Theory of Elasticity and Thermoelasticity*, North-Holland Series in Applied Mathematics and Mechanics, vol. 25, North-Holland Publishing Co., Amsterdam, 1979.
- [28] S. Lintner, O. Bruno, A generalized Calderón formula for open-arc diffraction problems: Theoretical considerations, *Proceedings of the Royal Society of Edinburgh* 145A (2015) 331-364.
- [29] Y. Liu, *Fast Multipole Boundary Element Method*, Cambridge University Press, New York, 2009.
- [30] Y. Liu, F. J. Rizzo, Hypersingular boundary integral equations for radiation and scattering of elastic waves in three dimensions, *Comput. Method Appl. Method Eng.* 107 (1993) 131-144.
- [31] F. Le Louër, A high order spectral algorithm for elastic obstacle scattering in three dimensions, *J. Comput. Phy.* 279 (2014) 1-18.
- [32] G. D. Manolis, D. E. Beskos, *Boundary element methods in elastodynamics*, Unwin Hyman, London, 1988.
- [33] J. C. Nédélec, *Acoustic and Electromagnetic Equations: Integral Representations for Harmonic Problems*, Springer-Verlag, New York, 2001.
- [34] M. S. Tong, W. C. Chew, Nyström method for elastic wave scattering by three-dimensional obstacles, *J. Comput. Phy.* 226 (2007) 1845-1858.
- [35] M. S. Tong, W. C. Chew, Multilevel fast multipole algorithm for elastic wave scattering by large three-dimensional objects, *J. Comput. Phy.* 228 (2009) 921-932.
- [36] T. Yin, G. C. Hsiao, L. Xu, Boundary integral equation methods for the two dimensional fluid-solid interaction problem, *SIAM J. Numer. Anal.* 55(5) (2017) 2361-2393.